FE-implementation of higher gradient theories and its use for experimental analysis

Wolfgang H. Müller Christian Liebold
wolfgang.h.mueller@tu-berlin.de

Abstract

It is well known that the material behavior at the micro- and (even more) at the nanoscale is size dependent, which is reflected, *e.g.*, in a stiffer elastic response. Therefore, Finite Element (FE) simulations of micro- and nanoelectromechanical systems should be able to incorporate the size effect. We focus on non-local theories, such as the couple stress and micro-polar theory for linear elasticity and implement the developed variational formulation in the open-source finite element code, called FEniCS®. Beam bending simulations with decreasing beam thicknesses were carried out. The material data and the geometries are in accordance with the experimental setup of Lam *et al.* (2003) [9] so that the numerical results are comparable to some experimental data. For a benchmark test of the numerical effectiveness an analytical solution for the one-dimensional Euler-Bernoulli beam theory was derived from the deformation energy density of couple stress theory. The final purpose of this procedure is to determine the material length scale parameter by an inverse analysis. The problem of boundary conditions for the additional derivatives of the displacement gradients and the strong dependence between the characteristic size of the finite elements and the intrinsic material length scale parameter are discussed.

1 Introduction

A quantitative understanding of a size effect in microstructures reflected in, for example, a stiffer elastic material behavior on the micro- and on the nanoscale is of great importance during modeling of micro- and nanoelectromechanical systems. A different deformation behavior on the micrometer scale has been observed first in metals and polymers deforming plastically, [15] and [6]. As far as a size effect in elasticity is concerned, Lam *et al.* (2003) [9] observed an increase in bending rigidities of micro-beams made of epoxy. The values for the bending rigidities were about 2.4 times larger than predicted by conventional theory if beam thicknesses decreased from 120 to 20 µm. McFarland *et al.* (2005) [12] have observed similar variations in the bending rigidities of polypropylene micro cantilevers. The corresponding loading was also within the linear elastic regime. Analogously other experiments have shown an apparent increase in YOUNG's modulus of elasticity without referring to non-local theories, [4] and [10]. Lam *et al.* (2003) [9] have shown that the elastic behavior of epoxy is independent of the thickness of the sample in the absence of strain gradients (for example, in uniaxial tensile tests). On the other hand a size effect in simple beam bending tests of the same samples (and thus in the presence of strain gradients) was observed.
Conventional theories based on the Boltzmann (or a.k.a. Cauchy) continuum are not able to predict the size effect. The so-called micro polar continuum theory, developed by [16], [13] and [5] originated from the work of E. and F. Cosserat (1909) [3], who introduced the idea of "point couples." Altenbach *et al.* (2010) [1] give a detailed history of the origin of

micro polar theories. In the present study, we interpret each material point of a deformable body as a particle that is able to undergo a microscopic rotation in addition to the macroscopic translation. Thus the balance of the angular momentum will completely uncouple from the balance of linear momentum. Rumor has it that this has even been anticipated in the very early days of mechanics, namely in the middle of the 18th century by Euler, Bernoulli and Lagrange (*cf.*, [17]). By connecting the intrinsic rotation to the macroscopic rotation vector, we are dealing with the Cosserat pseudo-continuum, also referred to as the couple stress model. Consequently, we have only one additional length scale parameter. Since second order derivatives of the displacements are taken into account, such theories violate the principles of local action and of simple bodies because the finite neighborhood will influence the deformation behavior of a certain material point.
In order to describe the size effect modified strain gradient theories have been developed until today. Moreover, so-called *methods of size effect* [8] have been defined in terms of a better experimental accessibility. By performing beam-bending simulations for slender micro-beams with decreasing thicknesses, we will use one of these methods here. Some research on the Finite Element Method (FEM) deals with the adjustment of special finite element formulations for the calculation and the evaluation of the second order displacement gradients in terms of the entire strain gradient theory, [18] and [2]. In contrast, the present study implements the couple stress theory of linear elasticity and is based consistently on the balance of linear momentum and on the independent balance of angular momentum. This will provide the possibility of a more or less rational justification of the size effect just by referring to the intrinsic rotations of the particles of a material. Influences of rotations on the material behavior also take part in the strain gradient and in the modified strain gradient theory.
The derived variational formulation is then built into the FEniCS® program. The novel open-source FE-software FEniCS® provides a collection of open-source packages for automated, efficient solutions of various differential equations, [11]. In this context, we take the impact of singular surfaces into account and include a jump of fields at the interfaces of the element.

2 Variational formulation

In our numerical study we start from the static balance of linear momentum and spin, without body-forces or body-couples. Following the summation convention for repeated indices, the divergence of the stress tensor, the associated constitutive law for the symmetric part of the force stresses and the balance of spin [9] read:

$$\sigma_{ji,j} = 0 \quad , \quad \sigma_{ij}^{\mathrm{sym}} = \lambda \varepsilon_{kk} \delta_{ij} + 2G\varepsilon_{ij} \quad , \quad \mu_{ji,j} + \varepsilon_{ijk}\sigma_{jk} = 0 \ , \tag{1}$$

where σ_{ji}, $\sigma_{ij}^{\mathrm{sym}}$, μ_{ji}, ε_{ijk}, ε_{ij}, δ_{ij}, λ and G are the so-called force stress tensor, the symmetric part of the force stress tensor, the couple stress tensor, the alternating tensor, the linear strain tensor, the KRONECKER delta, LAMÉ's constant and the shear modulus, respectively. We form the balance for the total angular momentum consisting of $\boldsymbol{x} \times \boldsymbol{v}$ and $\boldsymbol{s}$ (where $\boldsymbol{x}$, $\boldsymbol{v}$ and $\boldsymbol{s}$ are the vectors of the position, the velocity and the spin of the particle, respectively), which is a conserved quantity. Next, we assume static conditions, apply GAUSS' theorem and follow the rules of tensor calculus:

$$\frac{\mathrm{d}}{\mathrm{d}t}\int_M \left(\varepsilon_{ijk}x_j v_k + s_i\right)\mathrm{d}m = \oint_{\partial V} n_l \left(\varepsilon_{ijk}x_j\sigma_{lk} + \mu_{li}\right)\mathrm{d}A = \int_V \left(\varepsilon_{ilk}\sigma_{lk} + \varepsilon_{ijk}x_j\sigma_{lk,l} + \mu_{li,l}\right)\mathrm{d}V = 0 \ . \tag{2}$$

n_l denotes the surface normal of the volume surface and, in what follows, of the finite elements. In the balance of total angular momentum, Eqn. (2), the contribution of the

divergence of the stress tensor vanishes: The (static) balance of linear momentum implies that the divergence of the force stress tensor is zero. By multiplying the balance of linear momentum with arbitrary test functions of translation, δu_k, and the balance of angular momentum with test functions of rotation, $\delta\varphi_k$, which so far are independent of each other, both balances read:

$$\left.\begin{array}{c}\int\limits_V \sigma_{li,l}\delta u_i \mathrm{d}V = 0 \\ \int\limits_V (\varepsilon_{ilk}\sigma_{lk} + \mu_{li,l})\delta\varphi_i \mathrm{d}V = 0\end{array}\right\} \quad \int\limits_V (\underbrace{\sigma_{li,l}\delta u_i}_{(1)} + \underbrace{\mu_{li,l}\delta\varphi_i}_{(2)} + \varepsilon_{ilk}\sigma_{lk}\delta\varphi_i)\mathrm{d}V = 0\ . \tag{3}$$

Because of the arbitrariness and independence of both sets of test functions, the information contained in the original two equations is not affected by the summation. We transform the expression denoted by (1) in Eqn. (3) into a surface integral by means of Gauss' theorem. Hence, force boundary conditions in terms of the applied loads result. We also transform the expression (2) in Eqn. (3) with Gauss' theorem. Hence, we eliminate the derivative of third order of the displacement field in the couple stress tensor. Note that in anticipation of the finite element formulation Gauss' theorem is used in its more general form including jump terms:

$$\begin{aligned} 0 = &\int\limits_V \sigma_{li}\delta u_{i,l}\mathrm{d}V + \oint\limits_{\partial V} n_l(\sigma_{li}\delta u_i)\mathrm{d}A - \oint\limits_{A_\mathrm{s}} [\![\sigma_{li}\delta u_i]\!] n_l \mathrm{d}A_\mathrm{s} + \\ &- \int\limits_V \mu_{li}\delta\varphi_{i,l}\mathrm{d}V + \oint\limits_{\partial V} n_l(\mu_{li}\delta\varphi_i)\mathrm{d}A - \oint\limits_{A_\mathrm{s}} [\![\mu_{li}\delta\varphi_i]\!] n_l \mathrm{d}A_\mathrm{s} + \int\limits_V \varepsilon_{ilk}\sigma_{lk}\delta\varphi_i \mathrm{d}V\ . \end{aligned} \tag{4}$$

We now proceed to explain the importance of this formal procedure for FE: The volume V is decomposed into small subvolumes in which the field of the displacement (and, as we shall see, by coupling to the displacement also the rotation field) is approximated by polynomials. Now, since the force stress tensor and the couple stress tensor are related to the displacements and to the rotations by a constitutive law they will also be approximated polynomially. However, this way continuity of the displacement fields between the elements is not guaranteed yet, and needs to be accounted for by jumps of the form shown in Eqn. (4). We denote a jump by double parenthesis and assume the same material parameters in all finite elements. The nodes of two neighboring finite elements and their test functions for displacements, δu_k, are denoted with "+" and "-." The first jump $[\![\sigma_{li}\delta u_i]\!] n_l = (\sigma^+_{li}\delta u^+_i - \sigma^-_{li}\delta u^-_i) n^+_l$ is equal to zero, because the same test functions for displacements and the same displacement gradients $u^+_{i,j} = u^-_{i,j}$ lead to the same stresses at the interface of the neighboring elements.

From this point on, we replace the intrinsic rotation vector by the macroscopic rotation vector of the isotropic elasticity [7]: $\varphi_i = -\frac{1}{2}\varepsilon_{ijk}u_{k,j}$ and its variation $\delta\varphi_i = -\frac{1}{2}\varepsilon_{ijk}\delta u_{k,j}$. As a result of the coupling, the non-symmetric part of the force stress tensor, *i.e.*, the production of rotation in Eqn. (4) will cancel with a part of the first term: We decompose the stress tensor into its symmetric and its anti-symmetric part ($\sigma_{ij} = \sigma^{\mathrm{sym}}_{ij} + \sigma^{\mathrm{asym}}_{ij}$). By expanding it can be shown that $\sigma^{\mathrm{asym}}_{ij} = -\frac{1}{2}\varepsilon_{rij}\varepsilon_{rkl}\sigma_{kl}$. Thus, Hooke's law preserves its validity for representing force stresses. We insert the macroscopic rotation vector and the decomposition of the stress tensor into Eqn. (4) and get:

$$\begin{aligned} 0 = &\int\limits_V \left[\left(\sigma^{\mathrm{sym}}_{li} + \sigma^{\mathrm{asym}}_{li}\right)\delta u_{i,l} + \frac{1}{2}\varepsilon_{imn}\varepsilon_{ikl}\sigma_{kl} - \frac{1}{2}\mu_{li}\varepsilon_{imn}\delta u_{m,nl} \right] \mathrm{d}V + \\ &+ \oint\limits_{\partial V} \left[n_l\sigma_{li}\delta u_i - n_l\mu_{li}\frac{1}{2}\varepsilon_{imn}\delta u_{m,n} \right] \mathrm{d}A - \oint\limits_{A_\mathrm{s}} \frac{1}{2}\left(\mu^+_{li}\delta u^+_{m,n} - \mu^-_{li}\delta u^-_{m,n}\right) n^+_l \varepsilon_{imn}\mathrm{d}A_\mathrm{s}. \end{aligned} \tag{5}$$

The stress- and couple stress vectors acting on the boundary of the volume are denoted by $t_i = n_l \sigma_{li}$ and $m_i = n_l \mu_{li}$, respectively. The couple stress vector corresponding to an external load will be set equal to zero since in practice it is difficult to apply anyway. As shown in [9] the couple stress tensor is symmetric. By using the symmetric part of the rotation gradient χ_{ij}, which is deviatoric by nature:

$$\chi_{kl} = \frac{1}{2}\left(\varphi_{k,l} + \varphi_{l,k}\right) = -\frac{1}{4}\left(\varepsilon_{lij} u_{j,ik} + \varepsilon_{kij} u_{j,il}\right) \ , \tag{6}$$

the constitutive law for the couple stresses can be expressed as:

$$\mu_{lk} = 2Gl^2 \chi_{lk} = -\frac{1}{2} Gl^2 \left(\varepsilon_{lij} u_{j,ik} + \varepsilon_{kij} u_{j,il}\right) \ . \tag{7}$$

By exploiting the symmetry and the deviatoric nature of the rotation gradient there will be only be one additional parameter (namely $2Gl^2$, [7]) linking the couple stress to the rotation measure. If this parameter is set equal to zero the couple stress theory reduces to the conventional one. We utilize the strain tensor for small displacements $\varepsilon_{kr} = \frac{1}{2}\left(u_{k,r} + u_{r,k}\right)$ instead of $u_{k,r}$, and the rotation gradient tensor χ_{lk} instead of $-\frac{1}{2}\varepsilon_{lmn} u_{n,mk}$. Next, we write down the final variational form as follows:

$$0 = \int_V \left(\sigma_{li}^{\mathrm{sym}} \delta\varepsilon_{li} + \mu_{li} \delta\chi_{li}\right) \mathrm{d}V + \oint_{\partial V} t_k \delta u_k \mathrm{d}A - \oint_{A_\mathrm{s}} \frac{1}{2} [\![\mu_{li} \delta u_{m,n}]\!] \varepsilon_{imn} n_l \mathrm{d}A_\mathrm{s} \ . \tag{8}$$

The local form of Eqn. (8) lead to an elliptic partial differential equation of rank two.

3 Boundary conditions and implementation

Following a conventional three-dimensional elasto-static finite element analysis of a unilaterally clamped beam, we suppress the macroscopic motion and rotation of the entire finite element model by setting the displacements of the finite element nodes on the clamping surface equal to zero (implemented as Dirichlet boundary conditions). In particular, we incorporate no boundary condition for the microscopic rotation due to the direct coupling of the rotations. We apply the Galerkin method for spatial discretization to the expression shown in Eqn. (8). We have implemented the variational form in the context of the open source project FEniCS® and programmed a post-processing routine in the programming language python. For visualization, we used the open-source software Paraview-4®.
The mesh is built up by using equidistantly distributed tetrahedral continuous Lagrange elements with a polynomial degree of two corresponding to the rank of the resulting elliptic partial differential equation. The evaluation of the numerically calculated second order derivatives of the displacements is limited to just a few calculation points, and there is no interpolation in between. The routine of solving the system matrix is the method of Gaussian elimination (LU, for a lower / upper decomposition) with low effort in time. The material data is in agreement with the values for epoxy from [9]. These were reported to be $E = 3.8\mathrm{GPa}$, $\nu = 0.38$ and $l = 17.6\mu\mathrm{m}$. The material length scale parameter l had been determined by experiments.
The Poisson ratio ν for the constitutive law of the force stresses (Hooke's law) is assumed as zero in order to make the results of the three-dimensional FEM comparable to the Euler-Bernoulli beam theory (see Appendix). In general, the one-dimensional analytical model assumes a plane strain condition. For the material law of the couple stresses, we recalculate Young's modulus by $E^* = E(1-\nu^2)$ with the help of the transformation rules between plane stress and plane strain conditions. Thus we accommodate all the simplifications of the one-dimensional analytical solution (see Appendix). In addition, we utilize the shear modulus $G = E^*/(2+2\nu)$ for the constitutive law of the couple stresses,

as is widely done in literature on couple stress theory. The force F is applied in terms of a stress vector $t_k = (0, 0, -F/A)$ acting on the corresponding cross-sectional area A. The numerical accuracy of the iterative solution strategy has been set to a value of 1.0E-10 for the relative and for the absolute error tolerance, respectively.
We have changed the number of tetrahedral elements, however, without altering their aspect ratio (see Figure 1) and compared the maximum displacement u_z to the corresponding analytical result (see Appendix). When setting the material length scale parameter to zero, the deviation of the displacement u_z to the analytical results was about 0.1% for all different meshes. By setting the material length scale parameter non equal to zero the deviations of u_z to the analytical solution were approximately 0.8%. This value was only achieved for a mesh density, in which the edge length of the tetrahedral elements was two times the material length scale parameter itself. This implies a strong correlation between the size of the elements and the material length scale parameter. However, we did not investigate this correlation in detail. Some authors propose a correction factor that evaluates the ratio of the volume to the surface area of the different element sizes, [14].

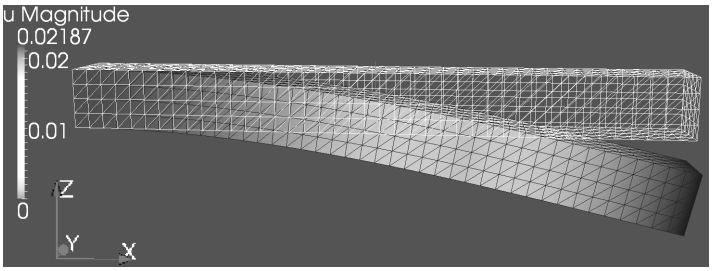

Figure 1: The mesh and an example of the deformation of an unilaterally clamped beam under the implementation of the Eqn. (8) in FeniCS®.

In the present study, the edge lengths of the elements correspond directly to the beam thicknesses, which also requires a minimum number of elements. For a proof that the additional influences of the rotations stem from strain gradients we also performed simulations of uniaxial tension tests. As a result, the u_x-values of the tension simulations (where no strain gradients are present) do not depend on the material length scale parameter.
We have structured the source code for the FE-simulations in terms of two objectives. First, we have simulated the bending rigidities of the beam while the dimensions of the beam were decreased. Figure 2 shows the corresponding results of the present FEM study. Second, for a constant beam geometry, but for different material length scale parameters we examined the deformation characteristics along the beam as follows: With the help of post-processing based on the numerical solution of the displacement field u_i we calculated the deflection curve (Figure 3, left), the y-component of the rotation vector (Figure 3, right):

$$\varphi_y = -\frac{1}{2}\varepsilon_{yjk}u_{k,j} \quad \text{with } j,k = x,y,z \ , \tag{9}$$

the strain in x-direction (Figure 4, left):

$$\varepsilon_x = u_{x,x} \ , \tag{10}$$

the equivalent strain (Figure 4, right):

$$\varepsilon_{\mathrm{VGL}} = \sqrt{\frac{2}{3}\varepsilon'_{ij}\varepsilon'_{ij}} \ , \tag{11}$$

(the prime refers to deviatoric strains) the yx-component of rotation gradient (Figure 5, left):

$$\chi_{yx} = -\frac{1}{4}\left(\varepsilon_{yij}u_{j,ix} + \varepsilon_{xij}u_{j,iy}\right) \quad \text{with } i,j = x,y,z \ , \tag{12}$$

and the equivalent couple stress (Figure 5, right):

$$\mu_{\mathrm{VGL}} = \sqrt{\frac{3}{2}\mu_{ij}\mu_{ij}} \ , \tag{13}$$

at specific evaluation points. These equidistantly distributed evaluation points were situated along a straight line of the axis of the beam. The line and the interspaces of the points we determined by fitting of the line to a position with minimal "noise" of the results. The resulting plots give information about some important deformation characteristics of the couple stress theory (*e.g.*, the rotation and the rotation gradient) and about the deviation of those from conventional theory (*e.g.*, the strain in x-direction).

4 Results

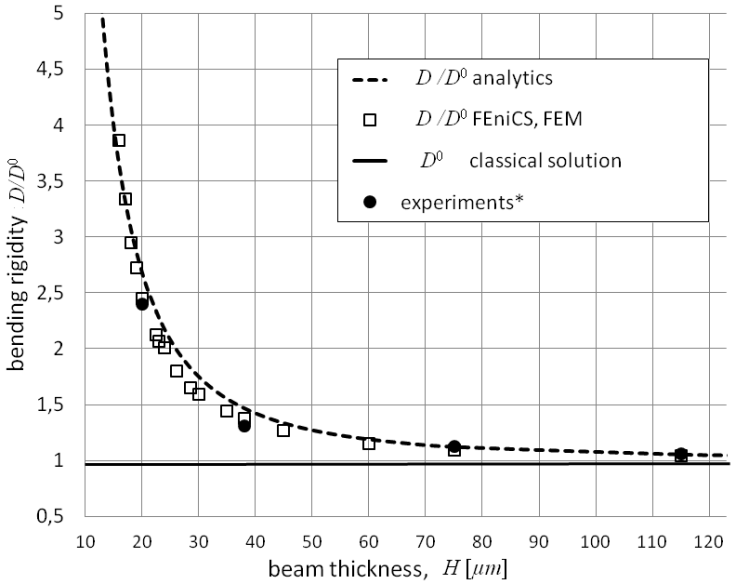

Figure 2: Normalized bending rigidities at different heights H of the beam. (*cf.*, Appendix, Eqn. (15))

The results for the increasing bending rigidities are in very good agreement to the results of the couple stress analysis based on the Euler-Bernoulli hypothesis (see Appendix) and to the experiments. The boundary condition at the fixed end of the beam causes some overestimate in the strain and rotation measures. The influence of Poisson's ratio results in a complex state of stress around the fixture. As mentioned above, only the constitutive law for the couple stresses depends on Poisson's ratio and thus this effect around the fixture is eminent for the equivalent couple stresses and for increasing material length scale parameters. As an unexpected result we, first, observe a reduction of the y-component of the rotation vector along the axial coordinate of the beam when increasing the material length scale parameter (see Figure 3, right). Second, the strains in x-direction behave non-linearly along the axial coordinate of the beam, whereas the equivalent strains stay linear. The reduction in the slopes of the equivalent strain distribution when increasing the material length scale parameters is in agreement to the predictions of one-dimensional beam theory (see Appendix, Eqn. $(14)_2$).

5 Appendix

Based on the strain energy density of the couple stress theory (*cf.*, [9]) we apply the Euler-Bernoulli assumptions of pure beam bending. By the principle of virtual work,

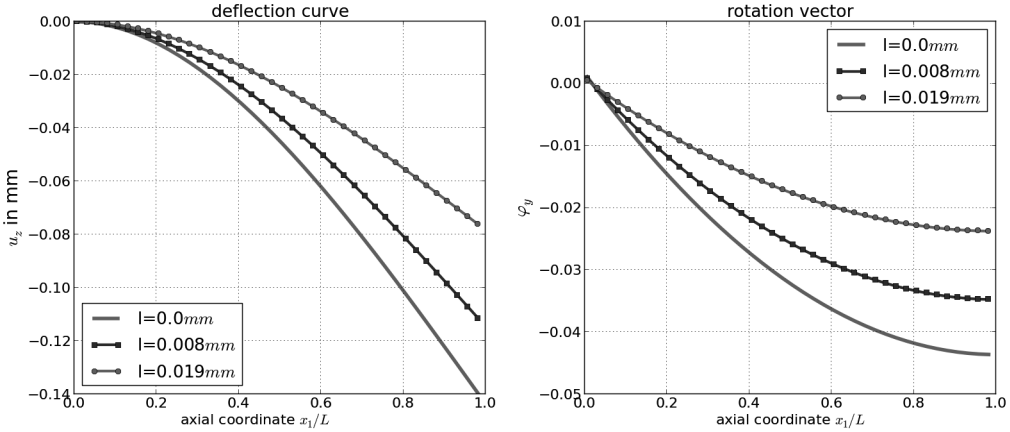

Figure 3: The deflection curve and the rotation vector, calculated at the equidistantly distributed points along a line in the interior of body. The beam geometry is: length-/width/height = 4800/30/30 μm, the force is F=1 μN, and the material data are for epoxy (see above).

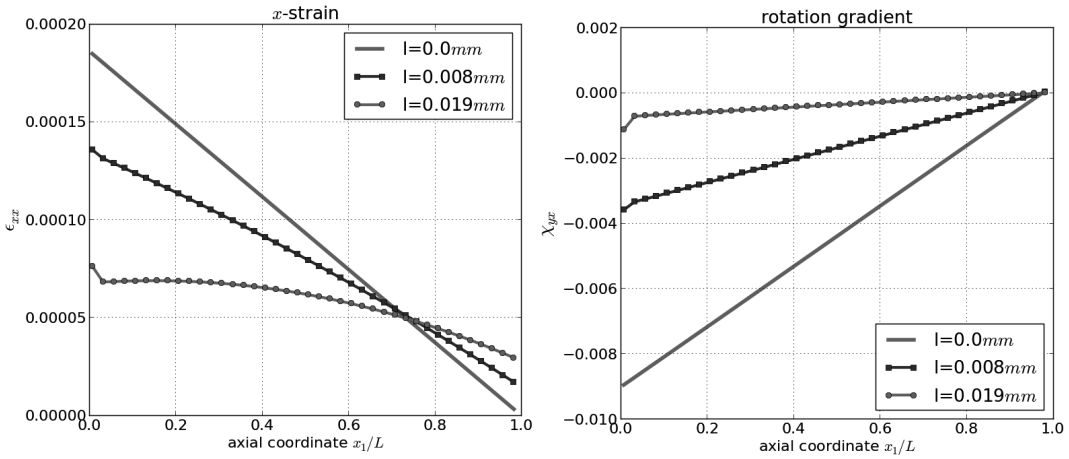

Figure 4: The strain in x-direction and the rotation gradient along the beam axis.

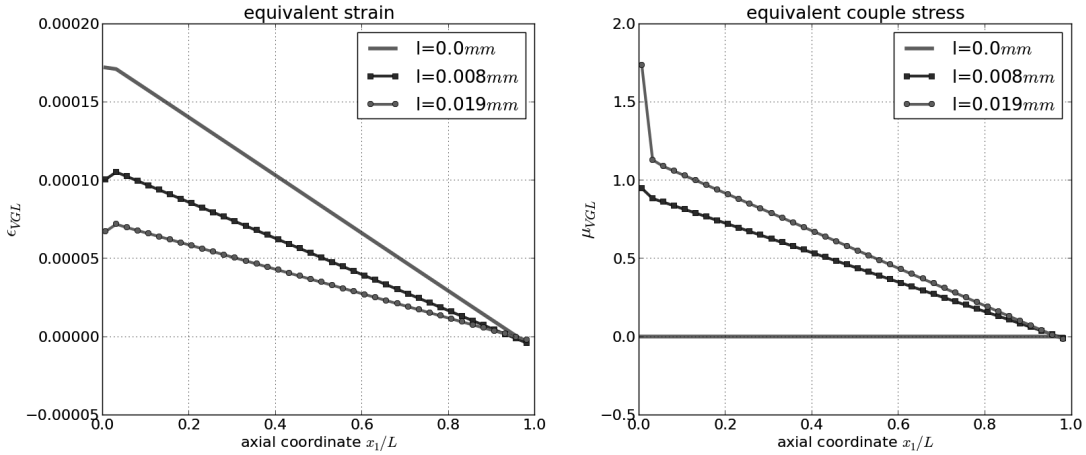

Figure 5: The equivalent strain and the equivalent couple stress along the beam axis.

the corresponding differential equation $\left(EI + \frac{1}{2}GAl^2\right) w^{\mathrm{IV}}(x) = q(x),\ \forall x \in (0, L)$ can be derived. By using as boundary conditions $Zw'''(L) = F$, $Zw(0) = 0$, $Zw'(0) = 0$ and $Zw''(L) = 0$, where Z is an expression for the bending stiffness, $Z = \left(EI + \frac{1}{2}GAl^2\right)$, the analytical deflection line and the analytical strains in x-direction read:

$$w(x) = -\frac{F}{\left(EI + \frac{1}{2}GAl^2\right)} \left[\frac{x^3}{6} - \frac{Lx^2}{2}\right] \ , \ \varepsilon_x = \frac{Fz}{\left(EI + \frac{1}{2}GAl^2\right)} [x - L] \ . \tag{14}$$

Here, we use the isotropic shear modulus, $G = E/(2 + 2\nu)$, without transformation of YOUNG's modulus between plain strain and plane stress condition. The bending rigidity from the couple stress theory, $D = F/w(L)$, is the ratio of the external force to the deflection of the point where the force acts. B and H denote the width and the height of the beam, respectively. Then, by comparison to the conventional bending rigidity, $D^0 = EI$, and by expanding the second moment of inertia, $I = BH^3/12$, and the area of the cross-section, $A = BH$, the normalized bending rigidity of couple stress theory reads:

$$\frac{D}{D^0} = \left(1 + \frac{3}{(1+\nu)} \left(\frac{l}{H}\right)^2\right) \ . \tag{15}$$

This formula additionally depends on the external beam dimension, H, as well as on the internal length scale parameter, l. This assures the ability of the present model to simulate the size effect by including a non-local theory.

Acknowledgements

The present work is supported by DFG MU 1752/33-1.

References

[1] Altenbach, J., Altenbach, H., Eremeyev, V.A. (2010). *On generalized Cosserat-type theories of plates and shells: A short review and bibliography.* Arch. Appl. Mech., **80**, pp. 73-92.

[2] Amanatidou, E., Aravas, N. (2002). *Mixed finite element formulations of strain-gradient elasticity Problems.* Comput. Methods Appl. Mech. Engrg. **191**, pp. 1723-1751.

[3] Cosserat, E., Cosserat, F. (1909). *Theorie des corps deformables.* Hermann et Fils, Paris.

[4] Cuenot, S., Fretigny, C., Demoustier-Champagne, S., Nysten, B. (2004). *Surface tension effect on the mechanical properties of nanomaterials measured by atomic force microscopy.* Physical Review B **69**, 165410.

[5] Eringen, A.C. (1976). *Continuum Physics. Vol. IV - Polar and nonlocal field theories.* Academic Press, Inc., New York.

[6] Guo, X.H., Fang, D.N., Li, X.D. (2005). *Measurement of deformation of pure Ni foils by speckle pattern interferometry.* Mechanics in Engineering, **27**(2), pp. 21-25.

[7] Kahrobaiyan, M.H., Asghari, M., Rahaeifard, M., Ahmadian, M.T. (2010). *Investigation of the size effect on the flexural characteristic of Timoshenko beams based on the couple stress theory.* International Journal of Engineering Science **48**(12), pp. 1985-1994.

[8] Lakes, R. (1995). *Experimental methods for study of Cosserat elastic solids and other generalized elastic continua*. Ed. H. Мьhlhaus, J. Wiley, N.Y., Ch. **1**, pp. 1-22.

[9] Lam, D.C.C., Yang, F., Chong, A.C.M., Wang, J., Tong, P. (2003). *Experiments and theory in strain gradient elasticity*. Journal of the Mechanics and Physics of Solids **51**(8), pp. 1477-1508.

[10] Li, X.-F., Wang, B.-L., Lee, K. Y. (2010). *Size Effect in the Mechanical Response of Nanobeams*. Journal of Advanced Research in Mechanical Engineering **1**(1), pp. 4-16.

[11] Logg, A., Mardal, K.-A., Wells, G. N. et al. (2012). *Automated Solution of Differential Equations by the Finite Element Method*. Springer [doi:10.1007/978-3-642-23099-8].

[12] McFarland, A.W, Colton., J.S. (2005). *Role of material microstructure in plate stiffness with relevance to microcantilever sensors*. Journal of Micromechanics and Microengineering, **15**(5), pp. 1060-1067.

[13] Mindlin, R.D., Tiersten, H.F. (1962). *Effects of couple-stresses in linear elasticity*. ARMA, **11**, pp. 415-448.

[14] Noels, L., Radovitzky, R. (2005). *A general discontinuous Galerkin method for finite hyperelasticity. Formulation and numerical applications*. Int. J. Numer. Meth. Engng. **68**(1), pp. 64-97.

[15] Poole, W.J., Ashby, M.F., Fleck, N.A. (1996). *Micro-hardness of annealed and work-hardened copper polycrystals*. Scripta Materialia, **34**(4), pp. 559-564.

[16] Toupin, R.A. (1962). *Elastic materials with couple-stresses*. ARMA, **11**, pp. 385-414.

[17] Truesdell, C. (1964). *Die Entwicklung des Drallsatzes*. ZAMM, **44**(4/5), pp. 149-158.

[18] Wei, Y. (2006). *A new finite element method for strain gradient theories and applications to fracture analyses*. European Journal of Mechanics A/Solids **25**, pp. 897-913.

W.H. Müller · C. Liebold
TU Berlin, Institut für Mechanik,
Lehrstuhl für Kontinuumsmechanik und Materialtheorie
Einsteinufer 5
10587 Berlin, Germany